Studying Higgs pair production in the process $\gamma\gamma \to H_0 H_0$ in the two-Higgs-doublet model

Sun La-Zhen and Liu Yao-Yang
Joint Institute of Eidgenössische Technische Hochschule & University of Science and Technology of China for High Energy Physics, Department of Modern Physics, University of Science and Technology of China, Hefei, Anhui, 230026, People's Republic of China
(Received 19 December 1995)

In the two-Higgs-doublet model the complete nonstandard Higgs boson helicity amplitudes for the Higgs boson pair production process $\gamma\gamma \to H_0 H_0$ is calculated and explicit formulas for nonstandard Higgs boson contributions to the helicity amplitudes are given. It is shown that the cross section is in the range of 0.03–30 pb at $\sqrt{s}=1$ TeV, for Higgs boson masses of $350 < M_{H_0} < 490$ GeV in monochromatic $\gamma\gamma$ collisions. The angular distribution for Higgs pair production is strongly peaked in the forward and backward directions. In particular the angular dependence for Higgs pair production is due to the nonstandard Higgs boson getting larger where the box diagrams constitute the dominant part of the differential cross section. For studying heavy Higgs pair production the use of circularly polarized photon beams with equal helicities is advantageous. [S0556-2821(96)04215-4]

PACS number(s): 12.60.Cn, 12.15.Lk, 14.80.Cp

I. INTRODUCTION

Since the discoveries of W and Z bosons, the standard model (SM) has been tested to high accuracy [1]. But, spontaneous symmetry breaking is not yet well understood, nor is there any experimental evidence to favor any particular symmetry breaking. The simplest model is the minimal standard model (MSM) with a single neutral scalar Higgs boson to activate the Higgs mechanism [2]. So far, direct searches have set a lower limit Higgs boson mass of about 60 GeV [1]. However, it is widely believed that the SM, despite its experimental success, cannot be complete and that new physics, beyond the SM, should be expected. One of the major goals of the next generation pp, e^+e^-, ep and the newly discussed $\gamma\gamma$ colliders is to search for the Higgs boson [3]. The Higgs boson of the MSM is still an explored area. A variety of options beyond the MSM are available to replace the job of the standard Higgs mechanisms. Among them, the model with a mild extension of the SM such as the two-Higgs-doublet models (THDM's) are constrained by the experimental value of $\rho = M_W^2/M_Z^2 \cos^2\theta_W = 1$ at the tree level [4] and by the strong limits on flavor changing neutral currents (FCNC's) [5]. The spectrum of physical states consists of a pair of charged Higgs bosons ($\Phi^{\pm}$), one neutral CP-odd pseudoscalar H_2, and two neutral scalar mix to form a pair of neutral CP-even scalars (H_0, H_1) with mixing angle α. The mixing angle β is given by $\tan\beta = V_2/V_1$, the ratio of the vacuum expectation values. The quantity $\tan\beta$ plays a central role in the theory because the couplings are often proportional to either $\tan\beta$ or $\cos\beta$. At the tree level the THDM is identical, in most respects, to the SM.

The reaction $e^+e^- \to H_0 H_0$ is studied [6]. It has a cross section decreasing as s^{-1}, which make it hardly observable even for $M_{H_0} \geqslant 100$ GeV. The $pp \to H_0 H_0$ via WW/ZZ fusion [7] has an increasing cross section, but still $\sigma \lesssim 10$ fb at $\sqrt{s}=40$ TeV for intermediate and heavy Higgs bosons ($M_{H_0} \geqslant 250$ GeV); therefore, in the hadron collider environment the process can hardly be studied. For renormalization group analysis, the larger the Higgs bosons mass, the lower the scale where new physics will appear [8]. Therefore, for heavy a Higgs boson one could expect to discover large deviations from the SM predictions.

The photon fusion process $\gamma\gamma \to H_0 H_0$ vanishing in the tree level has received much attention recently. The reason is that the emergence of a viable linear collider technique and the development of a high power laser suggests that the possibility to create high energy $\gamma\gamma$ collisions may become a reality [9]. Owing to the absence of large backgrounds, they yield a relatively clean environment for the exploration of the Higgs boson in the reaction $\gamma\gamma \to H_0 H_0$ and the search for new particles.

In this paper we present the complete nonstandard Higgs boson set of diagrams contributing to the process $\gamma\gamma \to H_0 H_0$ within the THDM. The MSM set of Feynmman graphs contributing to the process $\gamma\gamma \to H_0 H_0$ has been given in Ref. [10]. The neutral Higgs bosons H_0 have the same couplings as the MSM Higgs bosons, so that we can evaluate a meaningful nonstandard Higgs boson contributing within the THDM. We specify the THDM with $\tan\beta = V_2/V_1 \gg 1$, $\alpha = \beta$ and flavor-changing neutral currents at the tree level are avoided by one-Higgs-doublet (V_2) coupling to down-type quarks and charged leptons and the other (V_1) to up-type quarks. The minimal supersymmetric standard model belongs to this class, so our results also apply to this model.

II. THE $\gamma\gamma \to H_0 H_0$ HELICITY AMPLITUDES

The momenta and helicities of the incoming photon and outgoing H_0 bosons are defined through ($\lambda_{1,2} = \pm 1$)

$$\gamma(k_1, \lambda_1)\, \gamma(k_2, \lambda_2) \to H_0(p_1) H_0(p_2). \tag{1}$$

The Mandestam variables used in the following are given by

$$s = (k_1 + k_2)^2 = (p_1 + p_2)^2,$$

$$t = (k_1 - p_1)^2 = (k_2 - p_2)^2,$$

$$u = (k_1 - p_2)^2 = (k_2 - p_1)^2.$$

In the center of mass system (c.m.s.) of the photon photon the momenta read

$$k_{1,2}=\frac{\sqrt{s}}{2}\,(1;0,0,\pm 1), \tag{2}$$

$$p_{1,2}=\frac{\sqrt{s}}{2}\,(1;\pm\beta\,\sin\theta,0,\pm\beta\,\cos\theta). \tag{3}$$

θ is the scattering angle between the γ and the H_0 and $\beta=\sqrt{1-4M_{H_0}^2/s}$. In order to define helicity amplitudes we need to introduce the corresponding polarization vectors for different helicities in the c.m.s. of the initial photons are given by

$$\varepsilon_\mu(k_1,+1)=\varepsilon_\mu(k_2,-1)=\frac{1}{\sqrt{2}}\,(0;-1,-i,0),$$

$$\varepsilon_\mu(k_1,-1)=\varepsilon_\mu(k_2,+1)=\frac{1}{\sqrt{2}}\,(0;+1,-i,0).$$

Here ε_μ is the γ polarization vector with helicity ± 1. All momenta are taken to be on mass shell ($k_1^2=k_2^2=0, p_1^2=p_2^2=M_{H_0}^2$). The electromagnetic gauge invariance tells us that the $\gamma\gamma H_0H_0$ polarization tensor is transverse to the photon momenta:

$$k\cdot\varepsilon=0.$$

There are four helicity amplitudes, $\mu_{\lambda_1,\lambda_2},\lambda_1,\lambda_2=\pm 1$, of the process $\gamma\gamma\to H_0H_0$. CP invariance leaves only two independent ones; one has

$$\mu_{++}=\mu_{--}=G_0,$$

$$\mu_{+-}=\mu_{-+}=G_2,$$

two Lorentz and gauge invariant amplitudes $G_{0,2}$ contributing to the helicity amplitudes.

The normalizations are such that the helicity differential cross section is

$$\frac{d\sigma}{d\,\cos\theta}=\frac{\alpha^2\alpha_W^2}{2sM_W^4}\,(|G_0|^2+|G_2|^2)\,\frac{\beta}{16\pi}, \tag{4}$$

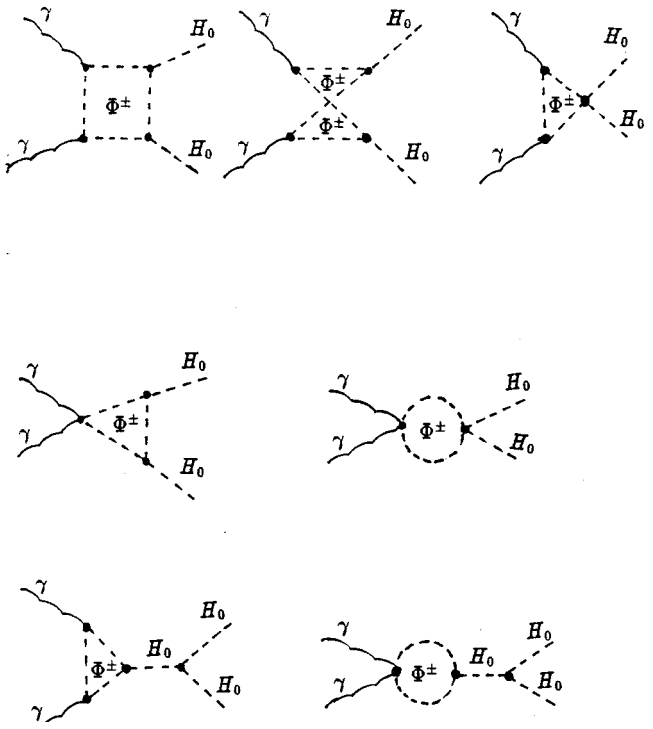

FIG. 1. The nonstandard Higgs bosons Feynman diagrams for the process $\gamma\gamma\to H_0H_0$ in the THDM. The graphs contributing to the nonstandard Higgs bosons $\Phi^\pm$ loops are marked by the symbols. The wavy lines present the initial photons; the dashed lines present the Higgs bosons. The graphs with the photon and Higgs permutations should be added when required.

where the parameters $\alpha=e^2/4\pi=1/128$, $\alpha_W=\alpha/s_W^2$, $s_W^2=1-M_W^2/M_Z^2$, $M_Z=91.188$ GeV, and $M_W=80.22$ GeV have been used throughout the paper and for our numerical analysis we have chosen $\tan\beta=70$ and $\tan\beta=10$ well within the limits listed in Ref. [11].

The nonstandard Higgs bosons diagrams of the process $\gamma\gamma\to H_0H_0$ in the THDM are presented in Fig. 1. The gauge-invariant subset for containing the usual box is labeled ''box,'' which contributes both to G_0 and G_2, and that containing the usual triangle is called ''triangle,'' which is nonzero only for equal photon helicities G_0. Each of the gauge-invariant subsets is separately finite. The determine the formulas for G_0 and G_2 the diagrams in Fig. 1 have to be calculated:

$$G_0(\text{triangle})=\frac{M_\Phi^2+\frac{A}{4}M_{H_0}^2\tan\beta}{s-M_{H_0}^2}\{(s-M_{H_0}^2)[B_0-2(C_{24}^{(1)}+C_{24}^{(2)})]+3[B_0-2(C_{24}^{(1)}+C_{24}^{(2)})]\}+(k_1\leftrightarrow k_2,t\to u), \tag{5}$$

$$G_0(\text{box})=-4\left(M_\Phi^4+\frac{A}{2}M_{H_0}^2M_\Phi^2\tan\beta+\frac{A^2}{16}M_{H_0}^4\tan^2\beta\right)\left\{2D_{27}^{(1)}+D_{27}^{(2)}+D_{27}^{(3)}+(s-4M_{H_0}^2)\,\frac{\sin^2\theta}{8}\,[2D_{23}^{(1)}+D_{11}^{(2)}-D_{13}^{(2)}+D_{21}^{(2)}\right.$$

$$\left.+D_{23}^{(2)}-2D_{25}^{(2)}+D_{12}^{(3)}+D_{22}^{(3)}]+\frac{1}{2}\,(C_0^{(1)}+C_0^{(2)})\right\}+(k_1\leftrightarrow k_2,t\to u), \tag{6}$$

$$G_2(\text{box}) = -\frac{(s-4M_{H_0}^2)\sin^2\theta}{2}\left(M_\Phi^4+\frac{A}{2}M_{H_0}^2M_\Phi^2\tan\beta+\frac{A^2}{16}M_{H_0}^4\tan^2\beta\right)$$
$$\times\{2D_{23}^{(1)}+D_{11}^{(2)}-D_{13}^{(2)}+D_{21}^{(2)}+D_{23}^{(2)}-D_{25}^{(2)}+D_{12}^{(3)}+D_{22}^{(3)}\}$$
$$+(k_1\leftrightarrow k_2, t\rightarrow u). \quad (7)$$

In these formulas $A=\tan 2\alpha$. The definition of the two, three, and four point functions B, C, and D can be found in Ref. [12]. The arguments of the invariant integrals are

$$B_0=B_0(k_1+k_2,M_\Phi,M_\Phi),$$
$$C_0^{(1)}=C_0(p_1+p_2,-p_1,M_\Phi,M_\Phi,M_\Phi),$$
$$C_0^{(2)}=C_0(-p_2,-p_1,M_\Phi,M_\Phi,M_\Phi),$$
$$C_{24}^{(1)}=C_{24}(k_1,-p_1-p_2,M_\Phi,M_\Phi,M_\Phi),$$
$$C_{24}^{(2)}=C_{24}(k_2,-p_1-p_2,M_\Phi,M_\Phi,M_\Phi),$$
$$D_{ij}^{(1)}=D_{ij}(k_2,k_1,-p_1,M_\Phi,M_\Phi,M_\Phi,M_\Phi),$$
$$D_{ij}^{(2)}=D_{ij}(-p_1,k_2,-p_2,M_\Phi,M_\Phi,M_\Phi,M_\Phi),$$
$$D_{ij}^{(3)}=D_{ij}(k_1,-p_2,k_2,M_\Phi,M_\Phi,M_\Phi,M_\Phi).$$

Using the methods of Ref. [12] C and D functions can be expressed in terms of Spence functions. Various checks were carried out to make sure that the resulting helicity amplitudes are correct. Cancellation of divergences, transversality to photon momenta, and symmetry under the interchange $t\leftrightarrow u$ were explicitly checked.

III. NUMERICAL RESULTS

A. Polarized cross sections for H_0H_0 pair production in monochromatic $\gamma\gamma$ collisions

We present the nonstandard Higgs bosons contributions to the polarized cross sections for H_0H_0 pair production in monochromatic $\gamma\gamma$ collisions. In order that an idealized case will provide a clear physical understanding the behavior of the double Higgs boson production, we consider here the extreme cases of $\lambda_1,\lambda_2=\pm 1$, i.e., full circular polarization for the incoming photons. All integrated cross sections are obtained from the angular range $9°\leqslant\theta\leqslant 171°$.

In Fig. 2 we present total cross sections for different polarization of the initial photon versus Higgs boson mass for $M_\Phi=200$ GeV at c.m. energies $\sqrt{s}=1$ TeV. The cross section is dominated by the charged Higgs boson loop contribution. The distinctive behavior of the cross section for large Higgs boson masses is the same as that observed for the W boson loop contribution in Ref. [10]. This is due to large coupling constants [present in Eqs. (5)–(7)] $\propto\alpha_W M_{H_0}^2/M_\Phi^2$ and $\propto\alpha_W M_{H_0}^4/M_\Phi^2$ of the virtual $\Phi^\pm$ and heavy H_0. The cross section lies in the range 0.03–30 pb for $M_{H_0}=350-490$ GeV and is much larger than that for the MSM contribution (in Ref. [10]).

The corresponding cross sections for the opposite photon helicities $\lambda_1=-\lambda_2=1$ are shown in Fig. 2. The cross section is contributed only by ''box'' diagrams. The cross section for opposite photon helicities is an order of magnitude smaller than that for equal photon helicities.

In Fig. 3 we show the angular distributions for Higgs pair production in the THDM for equal and opposite incoming photon helicities with $M_\Phi=200$ GeV, $M_{H_0}=250$, 350, and 450 GeV, respectively (at $\sqrt{s}=1$ TeV). We see the nonstandard Higgs bosons contribution to Higgs pair production is peaking in forward or backward directions for equal photon helicities, while the angular distributions for opposite incoming photon helicities is rather flat between 30° and 160° and smaller owing to the suppression of the t- and u-channel poles.

The angular dependence of the nonstandard Higgs bosons contribution to H_0 pair production for different M_Φ with $M_{H_0}=400$ GeV is plotted in Fig. 4 for $\sqrt{s}=1$ TeV, the dashed line is for $M_\Phi=150$ GeV, and the full line is for $M_\Phi=450$ GeV, respectively, (a) equal $\lambda_1=\lambda_2=1$ and (b) opposite $\lambda_1=-\lambda_2=1$ photon helicities. We see that the double Higgs production cross section grows with increasing M_Φ. The angular distributions shapes for opposite incoming photon helicities is difference between the SM [10] and THDM. The reason here is that the large nonstandard Higgs boson masses enhance contributions by the couplings of H_0 with Φ.

The effect of the large M_{H_0} mass is illustrated in Fig. 5. The angular distributions for equal and opposite initial pho-

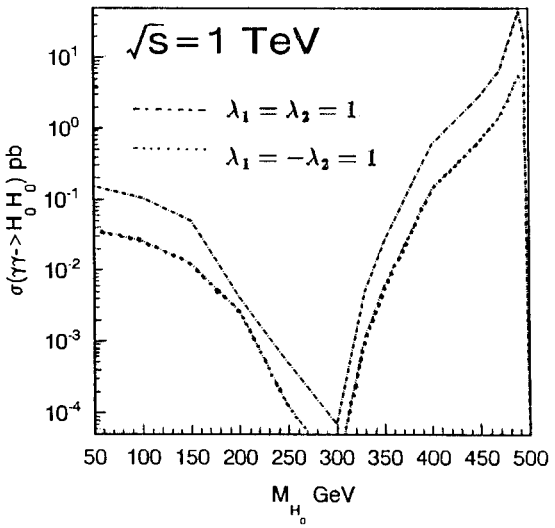

FIG. 2. The total $\gamma\gamma\rightarrow H_0H_0$ cross section at $\sqrt{s_{\gamma\gamma}}=1$ TeV for $M_\Phi=200$ GeV as a function of the Higgs boson mass. The dashed line is the total cross section for $\lambda_1=\lambda_2=1$. The dotted line is the total cross section for $\lambda_1=-\lambda_2=1$.

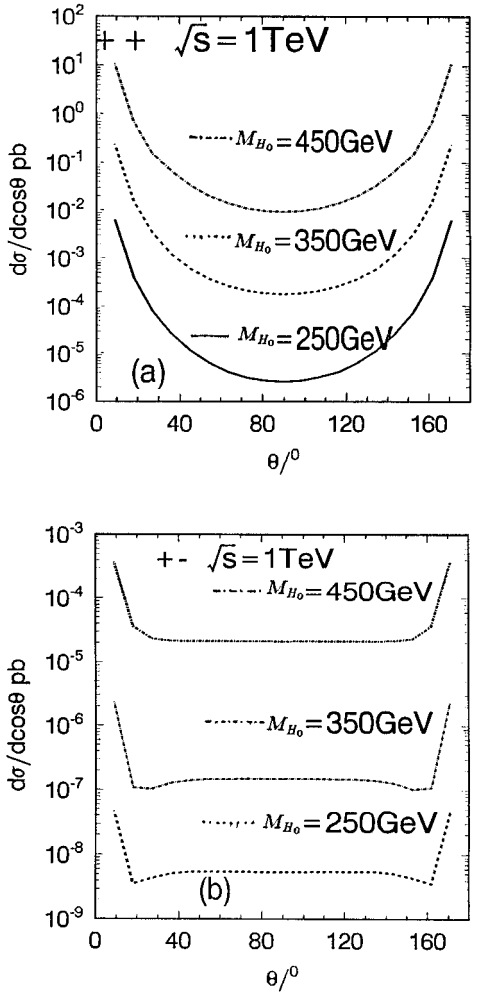

FIG. 3. The angular dependence of the differential cross section for the nonstandard Higgs bosons in the THDM and equal photon helicities (a) or unequal photon helicities (b) with M_Φ=200 GeV, M_{H_0}=250 GeV, M_{H_0}=350 GeV, M_{H_0}=400 GeV, and $\sqrt{s}$=1 TeV.

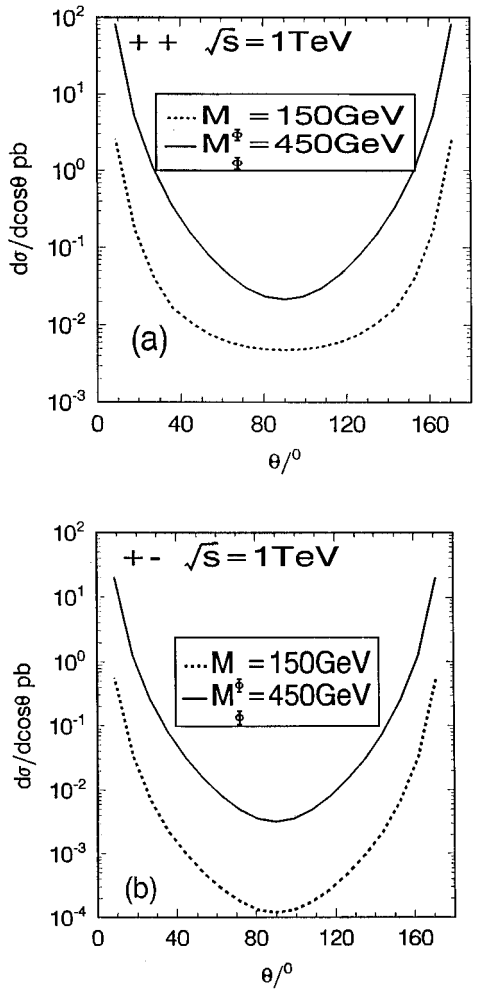

FIG. 4. Differential cross section for equal photon helicities (a) or unequal photon helicities (b) and $\sqrt{s}$=1 TeV at different values of the charge Higgs mass: M_Φ=150 and 450 GeV. The H_0 mass is M_{H_0}=400 GeV.

tons helicities is shown for different typical values of Higgs boson mass (M_{H_0}=400, 450, and 500 GeV, respectively) at $\sqrt{s}$=1.5 TeV and M_Φ=200 GeV. Enhanced H_0H_0 pair production at high energies for heavy Higgs boson mass was estimated in Ref. [10]. The heavier Higgs bosons mass, the larger is the differential cross section of its double production almost up to the kinematical boundary.

The origin of the large nonstandard Higgs boson contributions to double Higgs production is revealed in Fig. 6, where separate contributions to the differential cross section of the $\gamma\gamma\to H_0H_0$ are displayed for $\sqrt{s}$=1.5 TeV, M_{H_0}=500 GeV, and M_Φ=650 GeV both with (G_0(triangle)) and without (G_0(box),G_2(box)) the $H_0H_0H_0$ coupling. The box contributions to G_0 and G_2 have similar shapes. We see that there are no numerical problems for forward or backward Higgs production for opposite photon helicities where the cross section is equal to zero due to angular momentum conservation. From Fig. 6 we also see that for high energies and small or large scattering angles the differential cross section is dominated by the nonstandard Higgs bosons box graphs contribution. This is due to the fact that the nonstandard Higgs bosons triangle graphs contribution, for larger M_{H_0} (as M_{H_0}=500 GeV), is of order s^{-1} for all scattering angles. An analysis of the box contributions shows that these involve terms behaving as $1/|t|$ or $1/|u|$ for $M_\Phi^2 \ll |t| \ll s$ and approaching a constant of the order of $\alpha_W/\pi M_\Phi^2$ for $|t| \ll M_\Phi^2$. This behavior of the box contributions is familiar from many other (t-channel) processes. The process $\gamma\gamma\to H_0H_0$ is, however, that the triangle contribution does not exhibit a t or u pole. But even at a 90° scattering angle, the differential cross section for unequal photon helicities is smaller than the one for equal photon helicities by at least a factor of 10.

In Fig. 7 we give the nonstandard Higgs bosons contributions to the differential cross section of the H_0H_0 production for tanβ=10 and tanβ=70 with M_Φ=200 GeV and M_{H_0}=200 GeV at $\sqrt{s}$=1 TeV. As can be seen the sensitivity to the differential cross section is weak for tan $\beta \gg 1$.

B. H_0H_0 pair production at a photon linear collider

By Compton backscattering of laser photons off the linac electron or positron beams, one can produce high luminosity $\gamma\gamma$ collisions with a significantly harder $\gamma\gamma$ spectrum. In addition, a high degree of circular polarization for each of the colliding photons can be achieved by polarizing the incom-

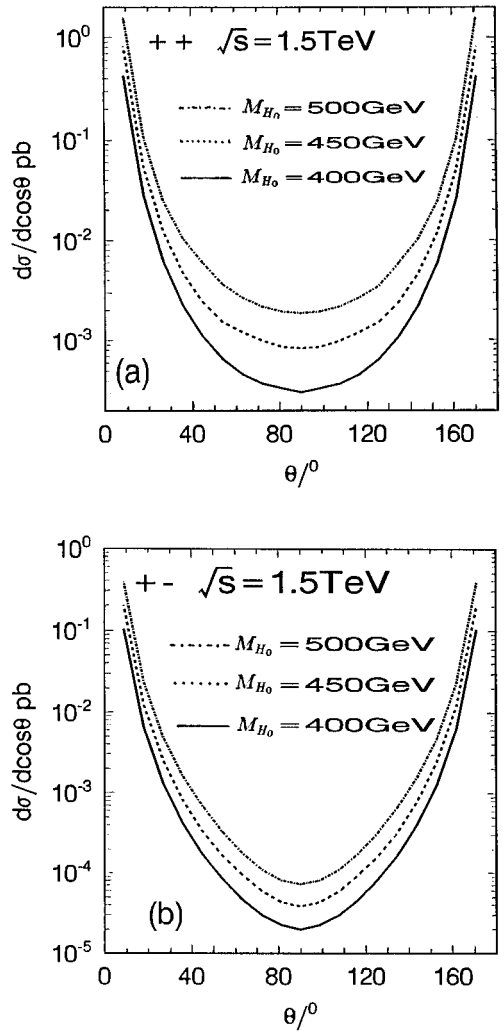

FIG. 5. Differential cross section for equal photon helicities (a) or unequal photon helicities (b) and $\sqrt{s}=1.5$ TeV at different values of M_{H_0}: $M_{H_0}=400$, 450, and 500 GeV. The Φ mass is $M_\Phi=200$ GeV.

ing electron or positron beams and laser beams [9]. The cross section of the H_0H_0 pair production in polarized $\gamma\gamma$ collisions is given by

$$d\sigma=\int_{4M_{H_0}^2/s}^{y_m^2} d\tau\,\frac{dL_{\gamma\gamma}}{d\tau}\left[\frac{1}{2}(1+\xi_1\xi_2)d\hat{\sigma}(++)\right.$$
$$\left.+\frac{1}{2}(1-\xi_1\xi_2)d\hat{\sigma}(+-)\right], \tag{8}$$

where photon photon luminosity is

$$\frac{dL_{\gamma\gamma}}{d\tau}=\int_{\tau/y_m}^{y_m}\frac{dy}{y}f_\gamma(x,y)f_\gamma(x,\tau/y),$$

$$\tau=\hat{s}/s,\quad y=E_\gamma/E_b,\quad y_m=\frac{x}{1+x},\quad x\equiv\frac{4E_b\omega_0}{m_e^2}. \tag{9}$$

Here E_b is the energy of the electron beam and ω_0 is the laser photon energy. The quantity y stands for the ratio between the scattered photon and initial electron energy and its maximum value is y_m. $\sqrt{s}(\sqrt{\hat{s}})$ is the $e^+e^-(\gamma\gamma)$ center of mass energy. The photon momentum distribution function $f_\gamma(x,y)$ and mean helicities of the two photon beams ξ_i are given by Eqs. (4) and (17) of Ref. [9]. The dimensionless parameter x is taken to be $x=2(1+\sqrt{2})$, which leads to the hardest possible spectrum of photons with a large luminosity. In the following we assume that 90% electron (positron) beam longitudinal polarization ($\lambda_{e1,2}=\pm0.45$) and 100% laser beam circular polarization ($\lambda_{\gamma1,2}=\pm1$) are achievable.

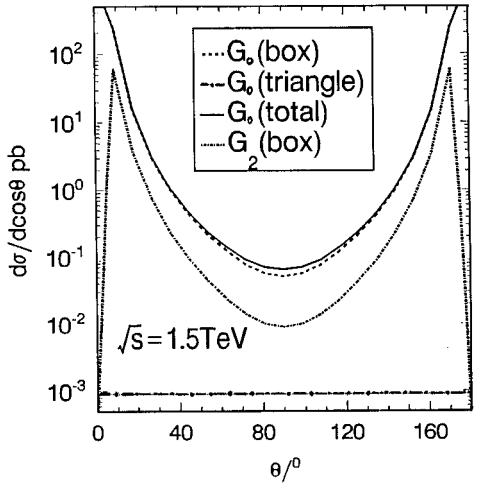

FIG. 6. The angular dependence of the pair Higgs bosons for $\gamma\gamma$ collisions at $\sqrt{s}=1.5$ TeV. The representative values $M_{H_0}=500$ GeV and $M_\Phi=650$ GeV have been chosen. The contributions of the different pieces are plotted separately.

In Fig. 8 we show the cross section of the H_0H_0 pair production at the photon linear collider (e^+e^- c.m.s. energy $\sqrt{s_{e^+e^-}}=1$ TeV) as a function of Higgs boson mass with $M_\Phi=200$ GeV. We consider different polarizations of the incoming electron (positron) and laser beams: $\lambda_{e1}=\lambda_{e2}=0.45$, $\lambda_{\gamma1}=\lambda_{\gamma2}=-1$ (the dashed lines in Fig. 8)

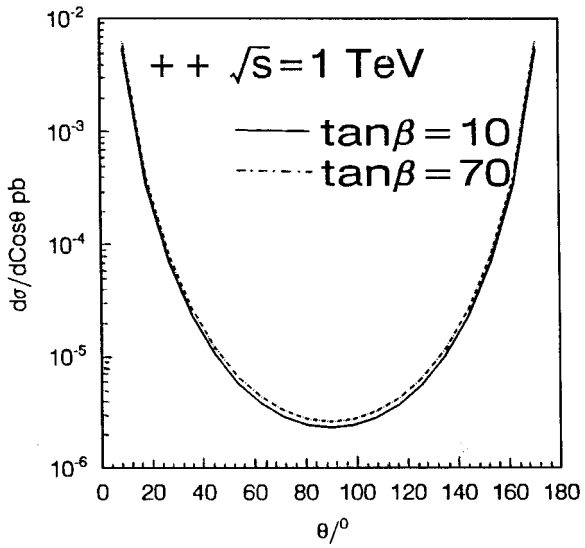

FIG. 7. The $\gamma\gamma\to H_0H_0$ differential cross section for equal photon helicities $M_{H_0}=200$ GeV, $M_\Phi=200$ GeV, and $\sqrt{s}=1$ TeV. The dot-dashed line and the solid line correspond to $\tan\beta=70$ and $\tan\beta=10$, respectively.

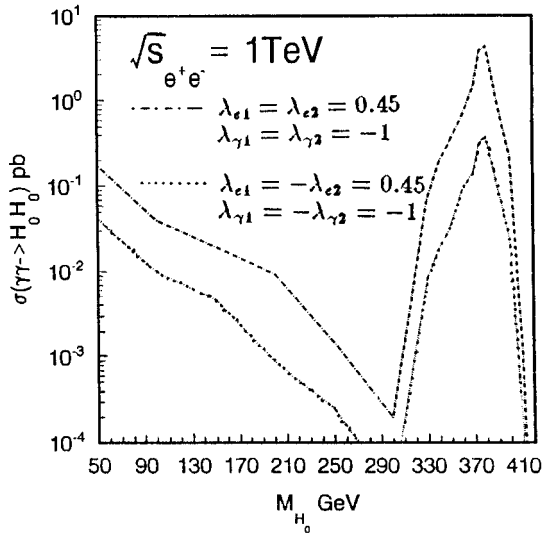

FIG. 8. The total $\gamma\gamma \to H_0 H_0$ cross section for laser backscattered photon in e^+c^- collisions at $\sqrt{s_{e^+e^-}}=1$ TeV as a function of the Higgs boson mass. Curves of the mean helicities of the incoming electron and laser beams $\lambda_{e1}=\lambda_{e2}=0.45$, $\lambda_{\gamma 1}=\lambda_{\gamma 2}=-1$, $\lambda_{e1}=-\lambda_{e2}=0.45$, and $\lambda_{\gamma 1}=-\lambda_{\gamma 2}=-1$ are shown.

and $\lambda_{e1}=-\lambda_{e2}=0.45$, $\lambda_{\gamma 1}=-\lambda_{\gamma 2}=-1$ (the dotted lines in Fig. 8). As for the case of monchromatic photon photon collisions the cross section peaking at large Higgs boson mass is observed. The cross section is smaller than that for the monchromatic photon spectrum and lies in the range 0.001–1 pb for $M_{H_0}=320$–400 GeV at $\sqrt{s_{e^+e^-}}=1$ TeV. For comparison, the double Higgs production cross section in MSM at the process $gg \to H_0 H_0$ is 1–10^{-3} pb for $50<M_{H_0}<250$ GeV and $m_t>40$ GeV for pp collision at $\sqrt{s}=40$ GeV [13] and WW fusion process $e^+e^- \to \nu\nu HH$ is 0.6–1.7 fb at $\sqrt{s}=1$–2 TeV for $M_H=25$ GeV [6]. Surely, the process $\gamma\gamma \to H_0 H_0$ will be the dominant mechanism for the double heavy Higgs boson production at future photon linear collider produced by the technique of the laser backscattering off electron linac beams.

IV. CONCLUSIONS

We have calculated the the nonstandard Higgs bosons contribution to process $\gamma\gamma \to H_0 H_0$ in the THDM. The double Higgs boson production in $\gamma\gamma$ collisions at TeV energies is feasible for studying at future $\gamma\gamma$ colliders, provided that the producing high energy photon beams by Compton backscattering of laser photons off high energy electrons will be realized to study photon photon collisions. The calculation shows that the cross section grows with increasing Higgs boson mass almost up to the kinematical boundary. This effect is due to the nonstandard Higgs boson loop contribution for which the triple and quadruple coupling with H_0 boson grow with increasing M_{H_0}. The cross section lies in the range 0.03–30 pb for $350<M_{H_0}<490$ GeV in monochromatic $\gamma\gamma$ collisions at $\sqrt{s_{\gamma\gamma}}=1$ TeV. Taking into account the real photon spectrum results in smaller cross section for heavy Higgs pair production. To estimate the event rates we have taken an integrated luminosity 10 fb^{-1} for a standard collider year, a thousand events per year would be observed. In order to observed these events, experimentally needs the detailed study of the background processes (the four gauge boson and two top quark pair production) in $\gamma\gamma$ collisions [10]. The angular distribution for $H_0 H_0$ pair production is strongly peaked in the forward and backward directions in monochromatic $\gamma\gamma$ collisions owing to the t- and u-channel poles at high energies and grows with increasing Higgs boson mass M_Φ and M_{H_0}. The dominating contributions of the differential cross section are from the nonstandard Higgs boson box graphs, which will always strengthen for the coupling of H_0 with heavy $\Phi^\pm$. The differential cross section for equal photon helicities is the larger than the one for opposite photon helicities. It is clear that to study heavy Higgs pair production and search for new particles the use of the equal photon helicities is advantageous.

ACKNOWLEDGMENTS

The work was supported in part by the Special Foundation for Doctoral Training of the National Education Committee of China under Grant No. 9435809 and the National Natural Science Foundation of China.

[1] J. Ellis, in *Proceedings of the Joint International Lepton-Photon Symposium and Europhysics Conference on High Energy Physics*, Geneva, Switzerland, 1991, edited by S. Hegarty, K. Potter, and E. Quercigh (World Scientific, Singapore, 1992); The LEP Collaborations, Phys. Lett. B **276**, 247 (1992).

[2] V. Barger and R. J. N. Phillips, *Collider Physics* (Addison-Wesley, Reading, MA, 1987); P. W. Higgs, Phys. Lett. **12**, 132 (1964); Phys. Rev. **145**, 1156 (1966).

[3] J. F. Gunion *et al.*, *The Higgs Hunter's Guide* (Addison-Wesley, Reading, MA, 1990).

[4] E. E. Boos and G. V. Jikia, Phys. Lett. B **275**, 164 (1992); B. S. Bertolini, Nucl. Phys. **B272**, 77 (1985).

[5] S. L. Glashow and S. Weinberg, Phys. Rev. D **15**, 1958 (1977); G. Marchio, R. Gutto, G. Sartor, and F. Strocchi, Nucl. Phys. **B163**, 221 (1980).

[6] V. Barger, T. Han, and R. J. N. Phillips, Phys. Rev. D **38**, 2766 (1988); **41**, 307 (1993); K. J. F.Gaemers and F. Hoogeveen, Z. Phys. C **26**, 249 (1984).

[7] W. Y. Keung, Mod. Phys. Lett. A **2**, 765 (1987); O. J. P. Eboli *et al.*, Phys. Lett. B **197**, 269 (1987); D. A. Dicus, K. J. Kallianpur, and S. S. D. Willenbrock, *ibid*. **200**, 187 (1988).

[8] G. Altarelli, in *'91 Electroweak Interactions and Unified Theories*, Proceedings of the 26th Rencontre de Moriond, Les Arcs, France, edited by J. Tran Thanh Van (Editions Frontieres, Gif-sur-Yvette, 1991), p. 443.

[9] I. F. Ginzburg *et al.*, Nucl. Instrum. Methods **205**, 47 (1983); **219**, 5 (1984); V. I. Telnov, Nucl. Instrum. Methods A **294**, 72 (1990).

[10] G. V. Jikia, Nucl. Phys. **B412**, 57 (1994); G. V. Jikia and Yu. F. Pirogov, Phys. Lett. B **283**, 135 (1992).

[11] L3 Collaboration, O. Adriani *et al.*, Phys. Rep. **236**, 1 (1993); W. Hollik, Z. Phys. C **37**, 569 (1988); J. F. Gunion and B.

Grzadkowski, Phys. Lett. B **243**, 301 (1990); D. Cocolicchio and J.-R. Cudell, *ibid*. **245**, 591 (1990); V. Barger, J. L. Hewett, and R. J. N. Phillips, Phys. Rev. D **41**, 3421 (1990); H. Huffel and G. Pocsik, Z. Phys. C **8**, 13 (1981); J. Maalampi, J. Sirkka, and I. Vilja, Phys. Lett. B **265**, 371 (1991).

[12] G. 't Hooft and M. Veltman, Nucl. Phys. **B153**, 365 (1979); G. Passarino and M. Veltman, *ibid.* **B160**, 151 (1979).

[13] E. W. N. Glover and J. J. Van der Bij, Nucl. Phys. **B309**, 282 (1988).